

# Characterization of mixing performance for bio-mimetic silicone cilia

Kieseok Oh · Brandon Smith · Santosh Devasia ·  
James J. Riley · Jae-Hyun Chung

Received: 23 November 2009 / Accepted: 28 January 2010 / Published online: 17 February 2010  
© Springer-Verlag 2010

**Abstract** This article presents the mixing performance of bio-mimetic cilia in a circular microchamber that is compatible with microwell plates. The mixing performance is characterized and compared with those of both diffusion- and vibration-induced mixers. To represent the mixing performance, the 90% mixing time, which was the time span for 90% mixing completion, was measured by analyzing the mixing process of black ink with water. The cilia mixer reduced the 90% mixing time by 8.0- and 1.4 times compared with those of the diffusion- and vibration mixers, respectively. In addition, the coefficient of variation of the 90% mixing time for the cilia mixer was reduced by 3.1- and 2.8 times compared with those of the diffusion- and vibration mixers, respectively. The experimental mixing performance was validated by numerical analysis. The simulations showed that the cilia mixer could significantly reduce the coefficient of variation because the convective flows generated by the cilia rapidly increased the surface area of the ink and thus rapidly decreased the variations in the initial mixing conditions.

**Keywords** Bio-mimetic cilia · Microfluidics · Micromixer · Resonance

**Electronic supplementary material** The online version of this article (doi:10.1007/s10404-010-0578-3) contains supplementary material, which is available to authorized users.

K. Oh · B. Smith · S. Devasia · J. J. Riley · J.-H. Chung (✉)  
Department of Mechanical Engineering, University  
of Washington, Seattle, WA 98195, USA  
e-mail: jae71@u.washington.edu

## 1 Introduction

Fluid mixing at the micro scale is challenging due to the relatively small Reynolds number of the flow; this Reynolds number represents the ratio of inertial to viscous effects. In such a laminar flow regime, the molecular mixing is governed by diffusion due to the low Reynolds number. To overcome this critical challenge, a number of microfluidic mixing methods have been demonstrated in the past decade. Such micromixing approaches are either passive or active depending on whether external input energy is present in the mixing process. Passive micromixers use grooves or specific geometries in order to generate chaotic advection and convective flows. Grooved patterns on the fluidic channel walls (Johnson et al. 2002; Stroock et al. 2002; Yang et al. 2005; Foley et al. 2008), obstacles in the fluidic path (Wang et al. 2002), and complex mixing channels (Bessoth et al. 1999; Therriault et al. 2003; Neils et al. 2004) have been effective in the microfluidic devices. The passive mixing approach is generally simple in fabrication but requires continuous flow by using syringe pumps or peristaltic pumps. Active micromixers use external energy to generate the complex flow field. Various kinds of external inputs, for example, acoustic waves (Liu et al. 2002; Yaralioglu et al. 2004), an electric field (Oddy et al. 2001; Sasaki et al. 2006), thermal energy (Tsai and Lin 2002), and a magnetic field (Lu et al. 2002; Qian and Bau 2005) have been employed to generate advective and convective flows and thereby enhance mixing. In spite of the relatively complex fabrication steps, the degree of the mixing could be adaptively controlled for a given geometry of microfluidic devices (den Toonder et al. 2008).

Bio-mimetic cilia and flagella approaches have been also studied for microfluidic mixing and manipulation.

Electrostatically driven cilia demonstrated the transport and mixing of fluids (den Toonder et al. 2008). The cilia composed of curled, polymer-coated chromium (Cr) microbeams were manipulated by an AC voltage to produce flows in the channel. The proposed device showed efficient mixing strategies in a Y-shaped channel device. Magnetic actuation could propel artificial flagella in fluid through propulsive flow generation (Dreyfus et al. 2005).

The major contribution of this article is to characterize a bio-mimetic micromixer that is compatible with microwell plates. Microwell plates containing an array of microwells are widely used for analyzing bio- and chemical reactions. A long-term goal of our research is to develop bio- and chemical reactors that are compatible with microwell plates using cilia mixers for high throughput bioassays.

In our previous study, a bio-mimetic cilia device composed of polydimethylsiloxane (PDMS) cantilevers was fabricated to generate fluid flows. The fabricated cilia mimicked the compliance and beating frequency of biological cilia. The cilia were resonated by sinusoidal excitation, which generated complex fluid flow in a fluidic channel (Oh et al. 2009). Although it was numerically found that such motion could be used for flow control and mixing enhancement (Khatavkar et al. 2007; Alexeev et al. 2008), it has not been clearly understood how the initial mixing conditions affect the mixing results and how the bio-mimetic cilia can enhance the mixing performance.

In this article, the PDMS cilia mixer is characterized by mixing black ink with deionized (DI) water. The mixing time and the uniformity of the cilia mixer in the presence of various initial conditions are compared with those of the mixers based on diffusion and vibration. The mixing efficiency is analyzed with relation to the initial mixing conditions of the ink aliquot in water using numerical simulation. In particular, the mixing performance of cilia- and diffusion mixers is

compared in order to evaluate the mixing efficiency in terms of the initial mixing conditions, including the location and perimeter of black ink in water.

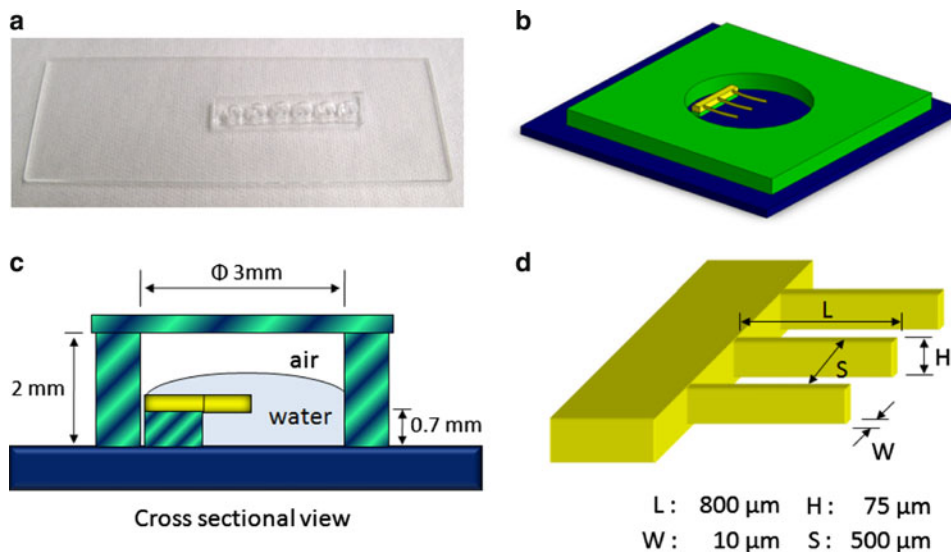
## 2 Experimental methods

### 2.1 Experimental configuration

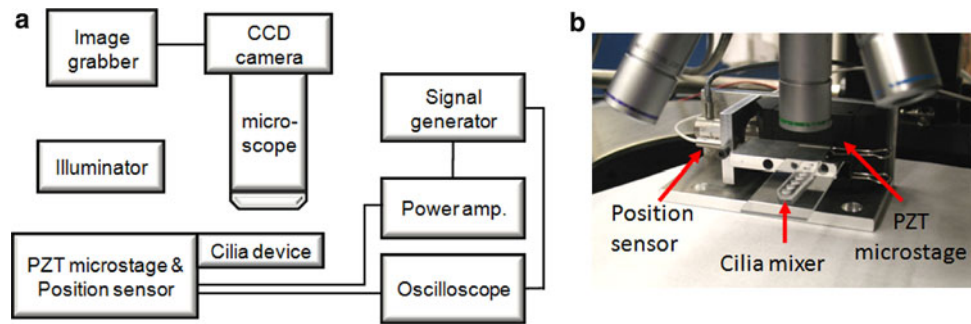
To characterize the mixing performance in terms of the mixing time and the degree of mixing, a cilia mixer was fabricated as illustrated in Fig. 1. The mixer was composed of a 1 mm-thick glass slide platform, a circular chamber, a supporting block, a cilia structure, and a cover plate. The circular chamber was made of a cured 2 mm-thick PDMS plate. The PDMS plate had a circular chamber whose diameter was 3 mm (Fig. 1c), which corresponded to the well diameter in 384-microwell plates. A 1.5 mm × 1 mm × 0.7 mm (W × D × H) PDMS block was prepared to support a cilia structure. In the chamber, three cilia having dimensions of 10 μm × 75 μm × 800 μm (W × H × L) were positioned with a spacing of 500 μm (Fig. 1d). To fabricate the PDMS cilia, a master mold was fabricated from a silicon wafer using photolithography, deep reactive ion etching (DRIE), and cleaning processes. PDMS prepolymer and curing agent (Sylgard 184, Dow Corning Corp.) were mixed and poured over the mold (Oh et al. 2009). After the curing, the cilia structure was peeled from the mold. An array of three cilia was cut under an optical microscope and then the cilia were placed on the support structure in the chamber. The cilia were bonded to the support structure by a PDMS thin layer. The chamber was covered with a 1 mm-thick PDMS plate.

Figure 2a shows a schematic of the experimental set-up for excitation of the cilia device. For the excitation, a lead–zirconate–titanate (PZT) microstage (PZS-200, Burleigh

**Fig. 1** Experimental configuration of a cilia mixer. **a** Picture of six cilia mixers. **b** 3-dimensional image of the cilia mixer. **c** Cross sectional view of a cilia mixer. **d** Cilia dimensions



**Fig. 2** Experimental set-up. **a** Schematics of the experimental configuration. **b** Cilia mixer that is clamped on a PZT microstage



Instruments, Inc.) was actuated by a signal generator (33220A, Agilent) through a high voltage amplifier (PZ-150M, Burleigh Instruments, Inc.). By manipulating the signal generator and the amplifier, the frequency and the excitation amplitude of the PZT microstage were controlled. The excitation amplitude of the cilia device was 10  $\mu\text{m}$ , which was confirmed by an inductive sensor (SMU-9000-15 N, Kaman Sensor Systems). An illuminator (Fiber-Lite MI-150, Dolan-Jenner Industries) was used as a light source. The cilia motion and the mixing process between water and ink were imaged through a charged coupled device (CCD) camera (DXC-390, Sony Electronics Inc.). The fluid flow induced by the cilia motion was traced by using polystyrene microspheres suspended in water. Figure 2b shows a cilia device that is clamped to the PZT microstage under a microscope.

## 2.2 Experimental procedure

To evaluate the performance of the cilia mixer, three approaches were used for mixing black ink in water. First, the cilia mixer was shaken by 10  $\mu\text{m}$  amplitude oscillations in the actuation direction orthogonal to the orientation of cilia. Second, the diffusion mixer was left without external agitation. Third, the vibration mixer was shaken by 10  $\mu\text{m}$ -amplitude oscillations without cilia in a chamber. The mixing performance of the three types of mixers was compared.

### 2.2.1 Frequency response test for a cilia mixer

To characterize the frequency response of the PDMS cilia in water, a 7  $\mu\text{l}$  aliquot of water was dropped in a circular chamber by using a pipette. The cilia, which were collapsed due to surface tension, were individually stretched by using tweezers. For massive production of the cilia assays, the underwater fabrication method could be used to avoid cilia collapse under surface tension (Oh et al. 2009). In this article, however, the cilia were manually stretched because a limited number of the cilia mixers were used for the characterization. The cilia mixer shown in Fig. 1 was excited by a PZT microstage. The sinusoidal input

frequencies were manipulated by a signal generator from 40 to 140 Hz by either 5 or 10 Hz increments to determine the resonance frequency. The excitation amplitude of the PZT microstage was 10  $\mu\text{m}$  for the frequency response test. At each frequency, the amplitude of a cilium was captured by a CCD camera and a light microscope. The capturing rate of the camera was 30 frames per second. The shutter of the camera was open and refreshed every 1/30 s. Thus, the imaging system could continuously trace the trajectory of cilia motion.

### 2.2.2 Tracking of microspheres for studying diffusion-, vibration-, and cilia-induced flow

To observe the flow pattern in the microchamber, a 0.5  $\mu\text{m}$  microspheres (mean diameter: 18.97  $\mu\text{m}$ , concentration: 0.1 mg/mL, Bangs Laboratories, Inc.) were added to a 6.5  $\mu\text{l}$  DI water solution. The cilia mixer was operated at a resonance frequency of 95 Hz with 10  $\mu\text{m}$  excitation amplitude. The motion of microspheres was video-captured and the video files were converted to sequential still images. The image files were analyzed through ImageJ and its plug-in software “MTrackJ” (Biomedical Imaging Group Rotterdam of the Erasmus MC—University Medical Center Rotterdam, Netherlands) in order to trace the paths of the selected microspheres. The same measurement procedure was conducted for the diffusion- and vibration mixers in order to compare the flow patterns. The diffusion mixer was left without external excitation. The vibration mixer was shaken without cilia at 95 Hz with 10  $\mu\text{m}$  excitation amplitude.

### 2.2.3 Mixing experiment using ink

The cilia mixer was clamped on the PZT microstage. The cilia mixer was positioned under a microscope to capture the video images of mixing progress through a CCD camera. An illuminator was used as an additional light source for enhancing image quality. After setting up the position of the cilia mixer, 6.5  $\mu\text{l}$  de-ionized (DI) water was dropped in the chamber using a pipette. The collapsed PDMS cilia were straightened by using tweezers. A 0.5  $\mu\text{l}$

aliquot of diluted black ink was gently dropped on the water aliquot using a pipette. The black ink (Drawing ink A, Pelikan, Hannover, Germany) was diluted with DI water by 1,500 times for the experiments. Considering the size of the chamber, 7  $\mu\text{l}$  was chosen as the total solution volume. In this addition of ink, the initial conditions, including the location and perimeter of ink on water, were inevitably changed due to the manual loading process of ink. Such uncertainty could not be rigorously controlled in our experimental configuration because surface interfacial energy dominant in microfluidics could not be precisely manipulated. After the addition of the black ink on DI water, the chamber was covered with a PDMS plate. To avoid evaporation of the solution, ambient temperature was cooled to 18°C by placing an ice pack around the cilia mixer. Subsequently, the PZT microstage was excited for cilia mixing. The whole mixing process was video-recorded for image analysis. The vibration mixing experiment was the same as the cilia experiment except that the cilia were not present in the chamber. Regarding the diffusion mixing, the experimental procedure was the same for the vibration mixing except that the chamber was not actuated. The cilia and vibration experiments were recorded for 10 min while the diffusion experiment was recorded for 30 min.

#### 2.2.4 Image processing method for mixing experiment

To quantify the magnitude of mixing from the captured images, Eq. 1 was used. This is an equation for the mixing index ( $I_{\text{mix}}$ ) at time  $t$  (Yang et al. 2005), which is a parameter indicating the mixing efficiency (Chang and Yang 2004). In Eq. 1, the progress of the mixing was estimated by the brightness of the pixels in a captured image. As the mixing progressed, the difference of the brightness was reduced, which increased  $I_{\text{mix}}$ . The images used in this analysis were composed of an array of 480 by 480 pixels with specific magnitudes corresponding to brightness. The brightness of each pixel was defined by the values between 0 and 256.

$$I_{\text{mix}}(t) = 1 - \frac{\sum_{i=1}^N |C_i(t) - C_{i\infty}|}{\sum_{i=1}^N |C_{i0} - C_{i\infty}|} \quad (1)$$

Here  $C_i(t)$  is the brightness of  $i$ th pixel at time  $t$ ,  $C_{i0}$  is the brightness of  $i$ th pixel at the initial time, and  $C_{i\infty}$  is the brightness of  $i$ th pixel at the final time.  $N$  is the number of pixels in the captured image.  $I_{\text{mix}}(t)$  is calculated at a given moment ( $t$ ).

For all the mixing experiments, the initial image was captured after the addition of ink on the water and the PDMS plate was covered. The last image was captured

when the fluid appeared to be fully mixed. The full mixing of fluid could be evaluated by visual observation with plotting the  $I_{\text{mix}}$  for the entire time range. After some time passed, the  $I_{\text{mix}}$  reached a plateau, meaning that the fluids were visually fully mixed because the difference between the current- and final image was no longer decreasing. At equilibrium, the  $I_{\text{mix}}$  did not reach 1 (fully mixed) because of the optical and thermal noise of the experimental setup. According to our experimental measurement, the peak-to-peak noise at full mixing was in the range of 10%. Considering the noise, the 90% mixing time ( $T_{90\% \text{mix}}$ ) was defined as the time span for 90% mixing completion.  $T_{90\% \text{mix}}$  was used for quantifying the mixing performance of the cilia-, diffusion-, and vibration mixers.

### 3 Numerical analysis

A numerical model was developed for understanding of the fluid flows generated by the cilia mixer. The computed flow field was used for analyzing the mixing performance of the cilia mixer. The mixing model including cilia was compared with the mixing model with diffusion alone in order to compare the mixing performance. In the simulation, the  $T_{90\% \text{mix}}$  was calculated for the cilia- and the diffusion mixing. The computed  $T_{90\% \text{mix}}$  was used for validating the experimental results.

The simulation was conducted by using COMSOL Multiphysics®. The simulation model consisted of two COMSOL simulation models: (1) a cilia-induced flow model and (2) a pure mixing model.

A two-dimensional flow simulation model was developed in the fluid–structure interaction mode of the micro-electro-mechanical-system (MEMS) module. The model was composed of the incompressible Navier–Stokes equations for flow analysis, plane strain analysis for structure deformation, and the arbitrary-Lagrangian–Eulerian (ALE) method for solving the moving boundary problem. The fluid flow in the model was described by Navier–Stokes equation and the continuity equation in order to solve for the velocity and pressure fields:

$$\rho \frac{\partial \bar{u}}{\partial t} - \nabla \cdot \left[ -p\bar{I} + \eta \left( \nabla \bar{u} + (\nabla \bar{u})^T \right) \right] + \rho (\bar{u} \cdot \nabla) \bar{u} = \bar{F} \quad (2)$$

$$\nabla \cdot \bar{u} = 0 \quad (3)$$

where  $\rho$  is the density of the fluid,  $\bar{u}$  is the velocity field,  $p$  is the pressure,  $\bar{I}$  is the unit diagonal matrix,  $\eta$  is the viscosity of the fluid, and  $\bar{F}$  is the cilia force acting on the fluid.



The structural deformation of cilia was calculated from the normal component of the fluid load:

$$L = \bar{n} \cdot \bar{L} = -\bar{n} \cdot (-p\bar{I} + \eta(\nabla\bar{u} + (\nabla\bar{u})^T)) \tag{4}$$

where  $\bar{L}$  is the load from the fluid, and  $\bar{n}$  is the unit vector normal to the structure boundary.

Figure 3a represents the geometry of the flow simulation model. The model contained three cilia having a cantilever of  $800 \mu\text{m} \times 10 \mu\text{m}$  with a  $500 \mu\text{m}$ -spacing in a circular chamber. The chamber had a 3 mm inner diameter and a 3.2 mm outer diameter. The cilia were attached to a supporting block. The height of the cilia was  $75 \mu\text{m}$  for computing fluid load on each cilium. The density of the cilia was  $980 \text{ kg m}^{-3}$  and the fluid density was  $1,000 \text{ kg m}^{-3}$ . The Young's modulus of the cilia structure was 2 MPa and the fluid viscosity was  $10^{-3} \text{ Pa s}$ .

Regarding the boundary conditions, the support and the chamber were excited in the x-direction with 95 Hz sinusoidal signal with  $10 \mu\text{m}$  amplitude. The cilia bases in the computational model were fixed at the support structure. The fluid load exerted on the cilia was computed from the velocity and pressure fields obtained from the solutions of the Navier–Stokes equations. No-slip boundary conditions were applied to all the boundaries in the fluid domain. Since the streaming motion induced by the resulting oscillatory flow was mainly of our interest, after the computation of the fluid model, the fluid velocity field was averaged over 10 periods in order to obtain the streaming flow field.

The mixing model was constructed in the convection and diffusion application mode of the MEMS module in COMSOL Multiphysics®. The concentration in the model was described by the convection–diffusion equation:

$$\frac{\partial c}{\partial t} + \bar{u} \cdot \nabla c = D\nabla^2 c \tag{5}$$

where  $c$  is the concentration of ink and  $D$  is the diffusivity of ink in water. The diffusivity ( $D$ ) in this computation was  $5 \times 10^{-10} \text{ m}^2 \text{ s}^{-1}$  (Lee et al. 2004). The time averaged fluid field calculated in the cilia-induced flow model was applied in the convective term. The mixing model was used to compare the mixing performance of the mixer with cilia to that of diffusion alone. Using the mixing model, the effects of the initial location and shape of the ink on the  $T_{90\% \text{mix}}$  were investigated.

Figure 3b–d shows the geometry of the mixing model. To analyze how the initial location and the shape (circle, ellipse 1, ellipse 2) of ink influence the  $T_{90\% \text{mix}}$ , three different locations and perimeters with the same area of ink were chosen. The area was  $0.283 \text{ mm}^2$ . The physical meaning of these parametric tests is that the same amount of ink is initially placed on a water aliquot with different perimeters and diffusion distances to the chamber boundary. The circular ink area (circle in Fig. 3b) had 0.6 mm in diameter with a perimeter (L1 in Fig. 3b) of 1.89 mm. The lengths of major axis and minor axis of the ellipse 1 (Fig. 3c) were 1.2 and 0.3 mm, respectively. The ellipse 2 (in Fig. 3d) had 1.8 and 0.2 mm in major and minor axis lengths, respectively. The perimeters of ellipse 1 (L2 in Fig. 3c) and ellipse 2 (L3 in Fig. 3d) were 2.75 and 4.02 mm. A1, A2, and A3 in Fig. 3b–d represent initial locations of ink. A1-circle was located in the center of the chamber. A2 and A3 were located by 0.5 and 1 mm in distance from the center in y direction.

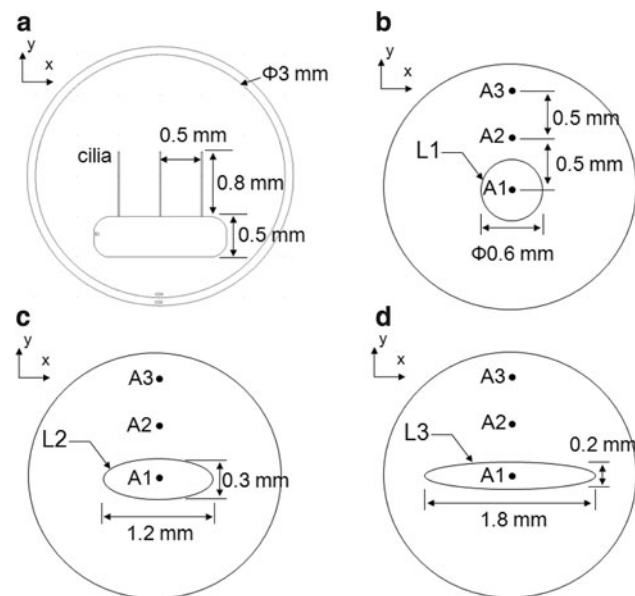


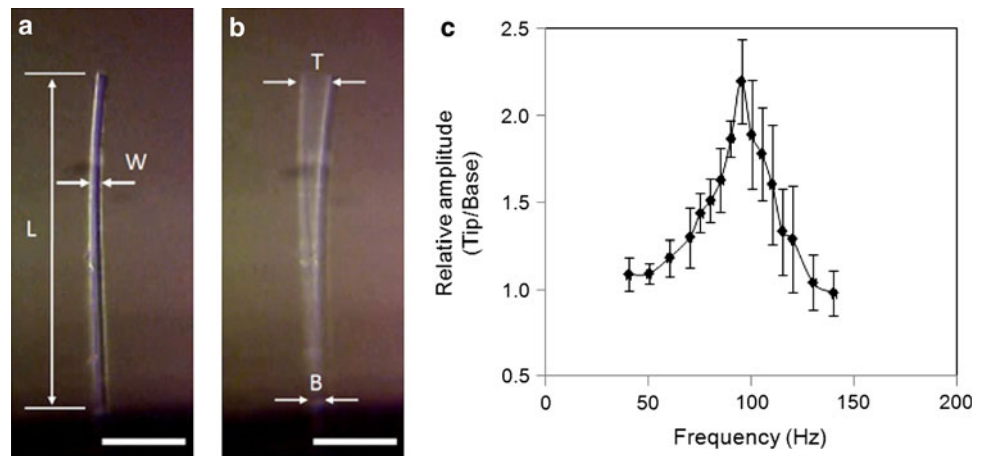
**Fig. 3** Simulation models. **a** Two-dimensional fluid flow model for a cilia mixer. **b–d** Two-dimensional mixing models containing different initial locations and perimeters of ink in a water domain

## 4 Results and discussion

### 4.1 Frequency response for a cilia mixer

Figure 4a shows a cilium in the mixer filled with water without excitation. ‘L’ and ‘W’ in Fig. 4a represent the longitudinal length and the width of the cilia, respectively. Figure 4b shows the resonance of a cilium at 95 Hz. In the figure, ‘B’ indicates the actuation distance of the cilium base and ‘T’ means the tip actuation distance of the cilium. The resonance behavior of cilia was studied by analyzing an added mass effect in our recent study. (Kongthon et al. 2009) In each still-image, the amplitude ratio (T/B) was measured with ‘ImageJ’ software (ImageJ, U. S. National Institutes of Health, Bethesda, Maryland, USA).

**Fig. 4** Characterization of the resonance frequency for a cilium in a cilia mixer. **a** A cilium in water without external excitation. The size of the cilium is  $800\ \mu\text{m} \times 10\ \mu\text{m} \times 75\ \mu\text{m}$  ( $L \times W \times H$ ). **b** Resonating cilium at 95 Hz. Scale bars:  $200\ \mu\text{m}$ . **c** Frequency response of the cilium in a cilia mixer filled with water. The error bars represent the standard deviation ( $n = 6$ )



#### 4.2 Tracking results of microspheres for cilia-, diffusion-, and vibration mixers

The paths of microspheres in the cilia, diffusion, and vibration mixers were observed for 10 s. Figure 5a presents the motion of microspheres in a cilia mixer. In the vicinity of the resonating cilia, microspheres were propelled into y-direction with circulation flows. Spiral and zigzag motion of microspheres was observed along the cilia. The propulsive flow at the cilia tip was circulated to the support structure of the cilia. In the diffusion mixer, microspheres barely moved in the chamber as shown in Fig. 5b. The vibration mixer could generate streaming flow in the chamber due to fluid oscillation (Fig. 5c) (Lutz et al. 2005). However, the cilia did not generate such complex flow at both lower (e.g., 40 Hz) and higher (e.g., 140 Hz) frequencies than the resonance frequency because of the low relative amplitude as shown in Fig. 4c. In the comparison with other mixers, the cilia mixer demonstrated more complex fluid flows, which could increase the interfacial

area between ink and water and significantly enhance the mixing performance.

#### 4.3 Experimental result of cilia-, diffusion-, and vibration mixers

Figure 6a–c shows sequential images of the mixing process for the cilia-, diffusion-, and vibration mixers. In the figures, water and ink are not present in the bottom area of the circular chamber due to hydrophobic PDMS material. Note that the terminal brightness of each experimental run could vary because of different illumination intensity as shown in Fig. 6a–c. However, the effect of the brightness difference for each run was eliminated by using the ratio of the brightness difference in Eq. 1. The cilia mixer showed the complete mixing at 180 s while the mixing was not completed for the diffusion mixer. When the cilia mixing was compared with the vibration mixing, the simple streaming flow of the vibration mixer separated the chamber fluid by half, which retarded the mixing process.

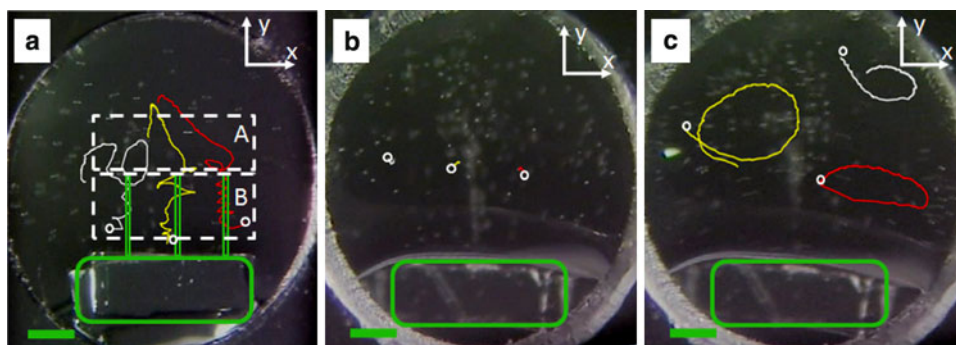


**Fig. 5** Paths of microspheres in cilia, diffusion, and vibration mixers. Circles represent the initial microsphere positions. Cantilevers and rounded rectangles indicate the cilia and the support, respectively. Dashed lines present areas for the flow velocity calculation area. Area A and B indicates above the cilia tip area and resonating cilia area,

respectively. Scale bars:  $500\ \mu\text{m}$ . **a** Microsphere paths for 10 s in a cilia mixer. **b** Microsphere paths for 10 s in a diffusion mixer. **c** Microsphere paths for 10 s in a vibration mixer. Video clips are available in the electronic supplementary materials

**Fig. 6** Captured images of the mixing process; **a** a cilia mixer, **b** a diffusion mixer, **c** a vibration mixer

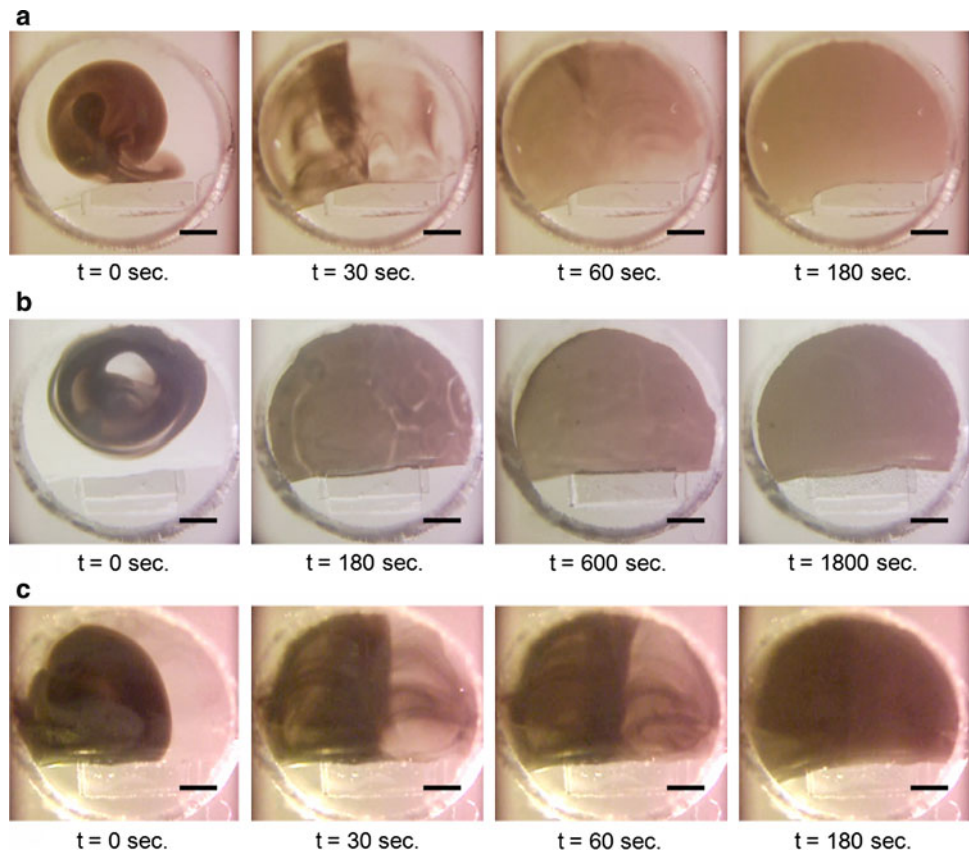


Figure 7a–c presents the variation of the mixing indices of the cilia, diffusion, and vibration mixers for six runs. Black circles in the graphs indicate the  $T_{90\%mix}$ . Red dashed lines in the figures represent the distribution of the  $T_{90\%mix}$ . The variations by the diffusion and vibration mixers were greater than that of the cilia mixer. The variation was caused by the different initial locations and shapes of ink drops as shown in Fig. 7d. The image (1) in Fig. 7d shows that an ink aliquot having a large interfacial length was located near the center of the chamber. The image (2) in Fig. 7d shows the smaller interfacial length with a further location of the ink aliquot from the chamber center. Thus, the  $T_{90\%mix}$  of the ink in image (1) was shorter than that of image (2).

The average  $T_{90\%mix}$  and the standard deviation for the six experiments are shown in Table 1. On average, the cilia mixer reached the 90% mixing at 81 s from the initiation of the mixing. The  $T_{90\%mix}$  of the cilia mixer was reduced by 8.0 times and 1.4 times compared to those of the diffusion- and vibration mixers, respectively. The vibration mixer generated streaming flows in the chamber (Lutz et al. 2005), which expedited the mixing compared to the diffusion mixer. However, the  $T_{90\%mix}$  of cilia mixer was shorter than that of the vibration mixer because the fluid flow in the chamber was much more complex. The complex flow significantly increased the interfacial length

between water and ink, which reduced the mixing time. It was hypothesized that the initial location and shape of ink in water could cause the large variation of the  $T_{90\%mix}$  for the diffusion and vibration mixers. The variations of the initial conditions were inevitably caused by the different potential energy and different location of ink aliquot in water. However, the cilia mixer could reduce the standard deviation by 24.8- and 3.9 times compared with the diffusion- and vibration mixers.

Figure 8 presents the comparison of mixing performance in terms of averaged  $T_{90\%mix}$  and a coefficient of variation (CV) of  $T_{90\%mix}$  for the cilia-, diffusion-, and vibration mixers. It was found that the coefficient of variation (CV) of  $T_{90\%mix}$  for the cilia mixer was reduced by 3.1- and 2.8 times compared with those of the diffusion- and vibration mixers, respectively. The significant reduction of the CV can improve the sensitivity and specificity of bioassays because the smaller CV increases a signal to noise ratio.

#### 4.4 Simulation results of cilia-induced fluid flow

Figure 9 shows the cilia motion in the fluidic chamber and the flow field of the cilia mixer computed by the numerical model. Propulsive flow was generated in the microchamber by the deflection of cilia (Purcell 1977; Dreyfus et al.

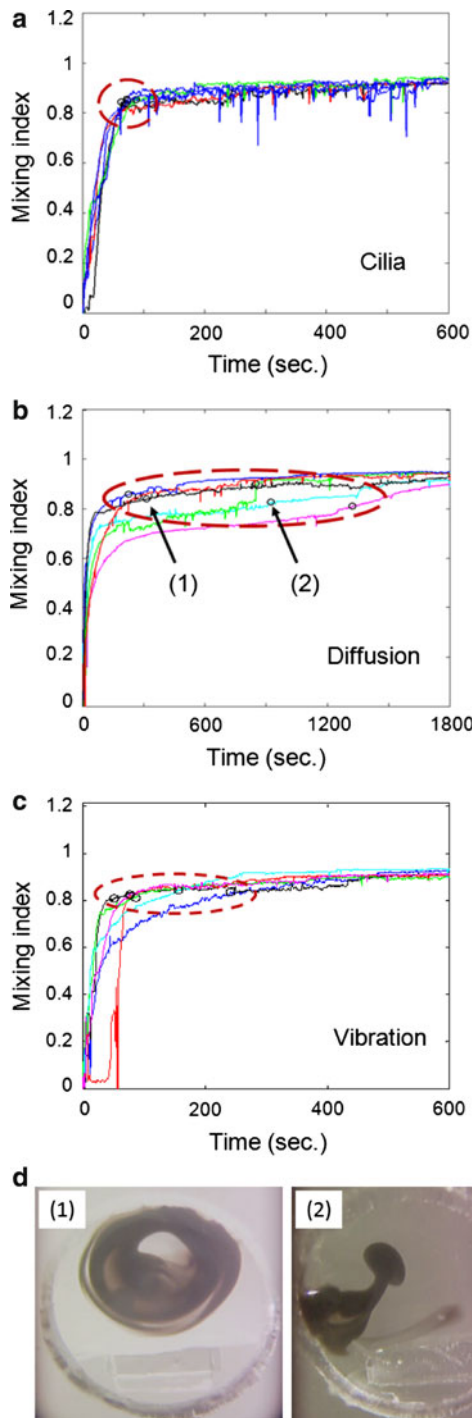


**Fig. 7** Experimental mixing results. Black circles in the graphs represent  $T_{90\%mix}$ . **a** Mixing index variation for the cilia mixer. **b** Mixing index variation for the diffusion mixer. **c** Mixing index variation for the vibration mixer. **d** Different initial locations and shapes of ink in a water aliquot.  $T_{90\%mix}$  of image (1) and (2) are indicated in the mixing indices for diffusion mixers (**b**)

2005). The velocity vectors in Fig. 9 were averaged over 10 periods because the flow velocity was continuously varying in an oscillatory manner due to the cilia motion. According to the simulation results, circulation flows were

**Table 1** Comparison of the experimental results for the 90% mixing time ( $T_{90\%mix}$ )

Mixing method	Average of $T_{90\%mix}$ (s)	Standard deviation of $T_{90\%mix}$ (s)
Cilia	81	18
Diffusion	651	447
Vibration	116	71

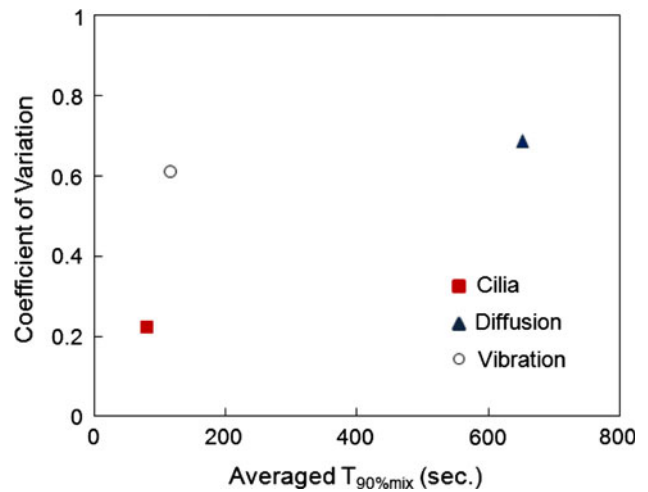


**Fig. 8** Comparison of the mixing performance for cilia-, diffusion-, and vibration mixers in terms of averaged  $T_{90\%mix}$  and coefficient of variation ( $n = 6$ )

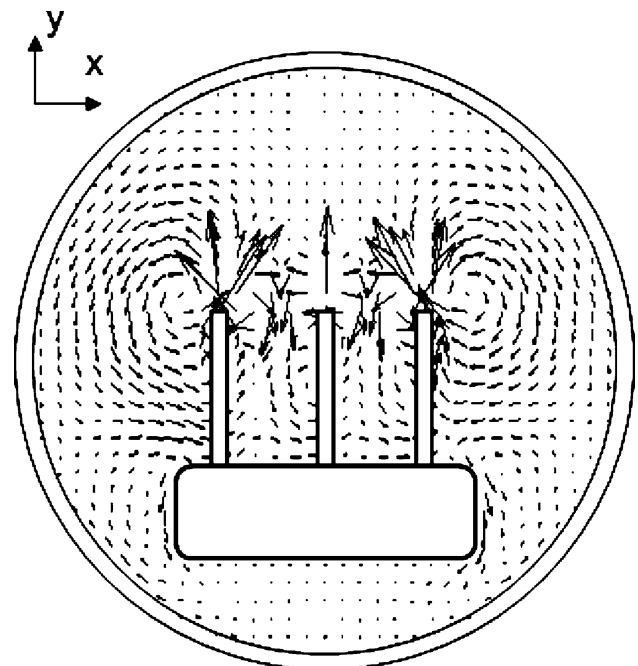
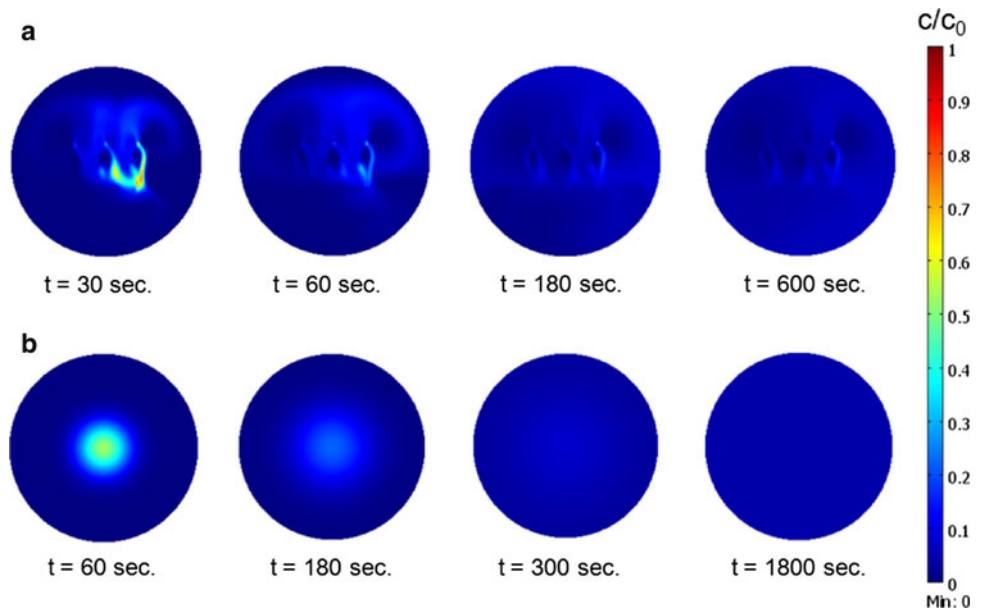


**Fig. 9** Cilia-induced fluid flow in a cilia mixer



**Fig. 10** Simulation results for cilia and diffusion mixers. **a** Simulation results of a cilia mixer. **b** Simulation results of a diffusion mixer



generated at the tip of each cilium and propulsive flows were created above the cilia. The result implies that the flow in the vicinity of cilia was directed in the y-direction with a wobbling motion in the x-direction. The computed average velocity near resonating cilia was  $107 \mu\text{m s}^{-1}$  in the y-direction and the average velocity above the cilia tip was  $82 \mu\text{m s}^{-1}$  in the y-direction. The experimentally measured averaged velocity in y-direction above the cilia tip (area A in Fig. 5a) was  $175 \mu\text{m s}^{-1}$ , and the y-velocity in the vicinity of resonating cilia (area B in Fig. 5a) was  $327 \mu\text{m s}^{-1}$ .

The experimental velocities were higher than those of the simulations. The difference could be caused by the smaller relative amplitudes of the cilia in the simulation and the free surface between air and fluid in the experiment. The relative amplitude of the simulation at 95 Hz was 1.5 while that of the experiment at 95 Hz was 2.1. The free surface motion in experiment could contribute to the amplification of the cilia motion, which was not considered in the simulation. In addition, the two dimensional analysis did not allow the simulation of out-of-plane directional flows. However, the directions of the in-plane velocity vectors agreed with those of the numerical results. Therefore, the velocity field could be used to help understand the mixing model in a qualitative way.

#### 4.5 Simulation results for cilia- and diffusion mixers

The results of the numerical model showed that the cilia motion generated local circulating flows that produced global flows, which enhanced the mixing by increasing the interfacial length between ink and water. Figure 10a, b presents the variation of the ink concentration in a chamber

for the cilia mixer at 30, 60, 180, and 600 s and for the diffusion mixer at 60, 180, 300, and 1800 s, respectively. Figure 10a shows that the mixing of ink in water can be significantly improved by the cilia in the mixer. Regarding the diffusion mixing, the black ink in the chamber is diffused to DI water as the mixing progresses (Fig. 10b). The diffusion required 382 s to obtain  $T_{90\%mix}$  for the circular-shaped ink located in the center of the chamber (case A1 with L1).

Figure 11a, b shows the variation of the mixing indices for the cilia and diffusion mixers with circular-shaped ink (L1) at different locations (A1, A2, and A3). The cilia mixer showed 80, 88, and 154 s for  $T_{90\%mix}$  according to the different locations with the standard deviation of 41 s. The values of  $T_{90\%mix}$  by the diffusion mixer were increased to 382, 500, 1060 s for the different locations of A1, A2, and A3, respectively. The different initial locations generated such a large standard deviation (362 s) because the diffusion distances from the initial locations to the circumference of the chamber were changed. The brighter color in the center of the chamber at 600 s in Fig. 10a showed the higher concentration, which was caused by the large difference of velocity vectors near the cilia structures. This higher concentration caused the smaller mixing index than 1 in Fig. 11a.

Figure 12 shows the  $T_{90\%mix}$  according to the different locations (A1, A2, and A3) and the perimeter lengths of ink (L1, L2, and L3) in water for the cilia- and diffusion mixers. The larger perimeter of the ink area could reduce the  $T_{90\%mix}$  because the large perimeter increased the interfacial length between ink and water, which enhanced the overall mixing. In addition, the initial location of ink could significantly affect the  $T_{90\%mix}$ . As the initial

**Fig. 11** Simulation results of mixing index variation. **a** Mixing index variation of a cilia mixer. **b** Mixing index variation of a diffusion mixer. Black circles represent  $T_{90\%mix}$

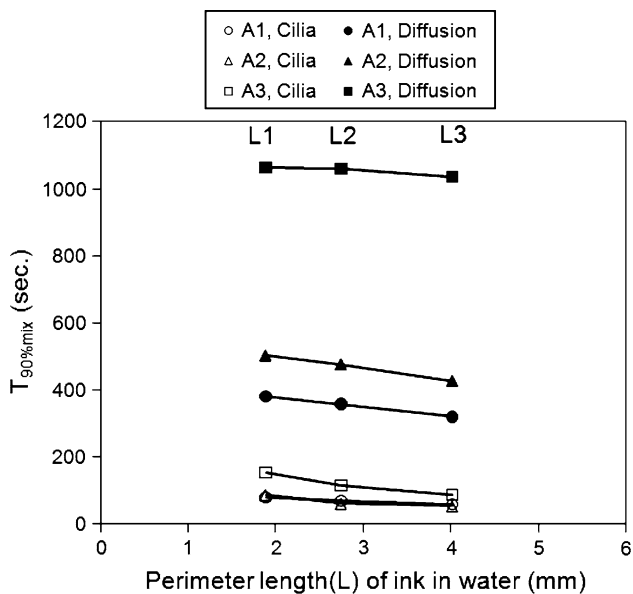
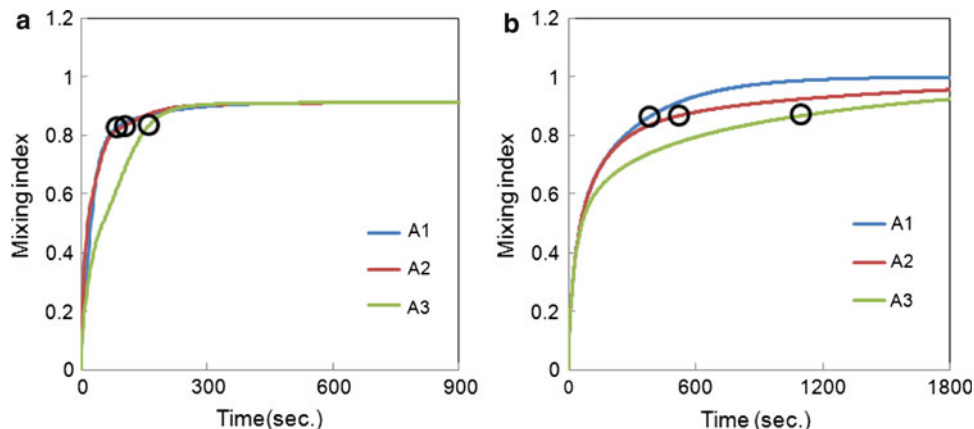


**Fig. 12** Simulation results: comparison of the 90% mixing time ( $T_{90\%mix}$ ) according to the various initial locations and perimeters

locations of ink became further from the center of the chamber, the diffusion distance was greater, which increased  $T_{90\%mix}$ . However, the cilia mixer could significantly reduce the  $T_{90\%mix}$  and its standard deviation because the interfacial length between ink and water was rapidly extended by the complex flow. These numerical results qualitatively support the experimental results for both the shorter mixing time and the smaller standard deviation of the cilia mixer compared with the diffusion mixer.

According to the experimental and simulation results, both the mixing time and the CV are reduced by using a mixer with cilia. To maximize the mixing performance, the length, spacing, and number of cilia should be optimized. The optimization goal can be addressed with the Sperm number (Sp). According to previous results (Dreyfus et al. 2005; Alexeev et al. 2008), the Sp for effective flow

generation is between 2 and 4. The Sp of our bio-mimetic cilia is 1.4, which should be further studied for effective mixing, in particular, in a limited chamber volume.

### 5 Conclusions

The mixing performance of bio-mimetic cilia mixer was experimentally characterized in comparison with those of the diffusion- and vibration mixers. The experimental results showed that the cilia mixer could reduce the 90% mixing time by 8.0- and 1.4 times compared with those of the diffusion- and vibration mixers. In addition, the coefficient of variation of the 90% mixing time for the cilia mixer was 0.2, which was smaller than those of the diffusion- and vibration mixers by 3.1- and 2.8 times, respectively. The numerical study showed that the 90% mixing time could vary because of the different initial locations and shapes of the ink in water. In the cilia mixer, the large variations were rapidly reduced by generating the complex flows. Therefore, compared with the diffusion- and vibration mixers, the cilia mixer could enhance the mixing and achieve much more uniform mixing results.

**Acknowledgments** This research was supported by the National Science Foundation (award number: CMMI 0624597) and the Royalty Research Fund at University of Washington.

### References

Alexeev A, Yeomans JM et al (2008) Designing synthetic, pumping cilia that switch the flow direction in microchannels. *Langmuir* 24:12102–12106  
 Bessoth FG, deMello AJ et al (1999) Microstructure for efficient continuous flow mixing. *Anal Commun* 36:213–215  
 Chang CC, Yang RJ (2004) Computational analysis of electrokinetically driven flow mixing in microchannels with patterned blocks. *J Micromech Microeng* 14:550–558

- den Toonder J, Bos F et al (2008) Artificial cilia for active microfluidic mixing. *Lab Chip* 8:533–541
- Dreyfus R, Baudry J et al (2005) Microscopic artificial swimmers. *Nature* 437:862–865
- Foley JO, Mashadi-Hossein A et al (2008) Experimental and model investigation of the time-dependent 2-dimensional distribution of binding in a herringbone microchannel. *Lab Chip* 8:557–564
- Johnson TJ, Ross D et al (2002) Rapid microfluidic mixing. *Anal Chem* 74:45–51
- Khatavkar VV, Anderson PD et al (2007) Active micromixer based on artificial cilia. *Phys Fluids* 19:13
- Kongthon J, McKay B, Iamratanakum D, Oh K, Chung JH, Riley JJ, Devasia S (2010) Added-mass effect in modeling of cilia-based devices for microfluidic systems ASME. *J Vib Acoust* 132(2): 1–7
- Lee S, Lee HY et al (2004) Ink diffusion in water. *Eur J Phys* 25: 331–336
- Liu RH, Yang JN et al (2002) Bubble-induced acoustic micromixing. *Lab Chip* 2(3):151–157
- Lu LH, Ryu KS et al (2002) A magnetic microstirrer and array for microfluidic mixing. *J Microelectromech Syst* 11:462–469
- Lutz BR, Chen J et al (2005) Microscopic steady streaming eddies created around short cylinders in a channel: flow visualization and Stokes layer scaling. *Phys Fluids* 17:7
- Neils C, Tyree Z et al (2004) Combinatorial mixing of microfluidic streams. *Lab Chip* 4:342–350
- Oddy MH, Santiago JG et al (2001) Electrokinetic instability micromixing. *Anal Chem* 73:5822–5832
- Oh K, Chung JH et al (2009) Bio-mimetic silicone cilia for microfluidic manipulation. *Lab Chip* 9:1561–1566
- Purcell EM (1977) Life at low Reynolds number. *Am J Phys* 45:3–11
- Qian S, Bau HH (2005) Magneto-hydrodynamic stirrer for stationary and moving fluids. *Sens Actuators B* 106:859–870
- Sasaki N, Kitamori T et al (2006) AC electroosmotic micromixer for chemical processing in a microchannel. *Lab Chip* 6:550–554
- Stroock AD, Dertinger SKW et al (2002) Chaotic mixer for microchannels. *Science* 295:647–651
- Therriault D, White SR et al (2003) Chaotic mixing in three-dimensional microvascular networks fabricated by direct-write assembly. *Nat Mater* 2:265–271
- Tsai JH, Lin LW (2002) Active microfluidic mixer and gas bubble filter driven by thermal bubble micropump. *Sens Actuators A* 97–98:665–671
- Wang HZ, Iovenitti P et al (2002) Optimizing layout of obstacles for enhanced mixing in microchannels. *Smart Mater Struct* 11: 662–667
- Yang JT, Huang KJ et al (2005) Geometric effects on fluid mixing in passive grooved micromixers. *Lab Chip* 5:1140–1147
- Yaralioglu GG, Wygant IO et al (2004) Ultrasonic mixing in microfluidic channels using integrated transducers. *Anal Chem* 76:3694–3698